Demonstration of Uncued Surveillance of LEO

Peter C. Zimmer
J.T. McGraw & Associates, LLC
Mark R. Ackermann
J.T. McGraw & Associates, LLC
University of New Mexico
John T. McGraw
J.T. McGraw & Associates, LLC
University of New Mexico

ABSTRACT

J.T. McGraw and Associates, LLC, in collaboration with the University of New Mexico (UNM), has built and is operating two proof-of-concept wide-field imaging systems to test novel techniques for uncued surveillance of LEO. The imaging systems are built from off-the-shelf optics and detectors resulting in a 350mm aperture and a 6 square degree field of view. For satellite streak detection, field of view is of critical importance because the maximum exposure time on the object is limited by its crossing time and measurements of apparent angular motion are better constrained with longer streaks. The current match of the detector to the optical system is optimized for detection of objects at altitudes above 450km, which for a circular orbit corresponds to apparent motions of approximately 1 deg./sec. Using our GPU-accelerated detection scheme, the proof-of-concept systems have detected objects fainter than V=12.3, which approximately corresponds to a 24 cm object at 1000 km altitude – at better than 6 sigma significance, from sites near and within Albuquerque, NM.

This work demonstrates scalable optical systems designed for near real time detection of fast moving objects, which can be then handed off to other instruments capable of tracking and characterizing them. The two proof-of-concept systems, separated by ~30km, work together by taking simultaneous images of the same orbital volume to constrain the orbits of detected objects using parallax measurements. These detections are followed-up by photometric observations taken at UNM to independently assess the objects and the quality of the derived orbits. We assert this demonstrates the potential of small telescope arrays for detecting and cataloguing heretofore unknown LEO objects.

1. FINDING AND TRACKING LEO OBJECTS WITH OPTICAL TELESCOPES

There has been increased interest in the potential for optical telescopes to make significant SSA contributions to the LEO volume. Optical techniques are not likely to supplant radar in the LEO regime, but can take advantage of some of the strengths of optical techniques. The principal advantage of optical SSA of LEO is that it is passive, using the Sun as the illuminator rather than having to project power. For radar this leads to the usual $1/R^4$ signal reduction because the projected power diverges both from transmitter to object and from object to detector. Optical telescopes are also relatively inexpensive, becoming more so every year, making them easily and cost effectively deployable around the world. Compared to radar the most significant shortcoming of optical techniques for uncued LEO SSA are that the Sun illuminates LEO for only a few hours per day and are not effective under moderate cloud cover. Depending on the observatory site and the altitude within LEO (lower altitudes are illuminated in terminator for less time than higher ones), this can easily lead to a coverage factor in the range of 5-10%. The work presented here is adding to the case that that small telescopes (by which we mean meter-class or smaller) can rapidly and robustly detect small objects (10cm or smaller) and thus should be seriously considered for the SSA portfolio.

In the next section, we will summarize the scope of observing objects in LEO orbits with ground-based optical sensors. Section 3 details the hardware we have deployed to serve as a proof of concept and test bed for our techniques. Section 4 presents a small sample of the type of data and detections that have been made with these systems. Section 5 reports on some preliminary measurements of parallax range using our two optical systems together. Section 6 offers some suggestions about the possibilities and potential of larger telescopes systems.

2. SIGNAL-TO-NOISE OF FAST MOVING OBJECTS – AN OVERVIEW

We have previously detailed the challenges and scope of the problem of detecting small objects in the LEO volume using wide field optical telescopes (Ackermann et al. 2003 [1]) and the particular approach we use for detecting the streaks they leave in images (Zimmer, Ackermann and McGraw 2013 [2]). The relevant highlights of this are:

- Objects in LEO are bright by astronomical standards
  - A 10cm object at 1000km ~12th magnitude (A=1) to 14th magnitude (A=0.12)
  - A golf ball (4.2cm) at 1000km range with a 90% albedo is ~14th magnitude
  - Even under bright skies, 16th magnitude is bright enough to detect in 1s with a 300mm telescope
- Objects in LEO have a high apparent angular velocity
  - ~0.2 deg/s at 2000km, 0.4 deg/s at 1000km, and up to ~1.5 deg/s at 300km, observed near zenith
  - Light from LEO objects is therefore trailed over many pixels, each contributing noise – so-called trailing losses
  - The resulting loss in per-pixel signal-to-noise ratio scales as the number of pixels in the streak, which can be hundreds to thousands of pixels long
- Signal-to-noise in the whole LEO streak is more significant by approximately the square root of the streak length
  - <u>If you can find it in the first place.</u>
  - The low per-pixel S/N is most often ignored as part of the background by traditional source detection techniques because the per kernel S/N does not cross a statistical significance threshold
- Rapid cadence (~1s) imaging with zero deadtime of wide instantaneous fields of view (FOV >> 1 square degree) can catch LEO objects as they streak through the field
  - Exposure time tailored so that a 1 deg/s object will cover half of the short dimension of the FOV
  - Zero deadtime for maximum efficiency and no lost objects between exposures
  - Optimize for existing hardware, minimum read noise and feasibility of real time detection
- No need to track – for the short exposures we use, we can allows stars to trail without reducing effective system coverage of the LEO volume

These factors have guided the overall development of our hardware and software techniques and represent one set of solutions to detect faint objects in LEO orbits given real world constraints and conditions. Detector technology and computer hardware capabilities continue to grow exponentially and these trends only serve to make optical SSA of LEO more effective and affordable.

3. DEPLOYMENT AND TESTING OF PROOF-OF-CONCEPT SYSTEMS

The initial phase of this work investigated available COTS telescopes systems to try to find the most cost-effective telescope system to provide a real demonstration and test bed for our techniques. Available detectors are consistently the limiting factor. Our budgetary constraints effectively eliminated backside illuminated CCDs, which are desirable for their high quantum efficiency, though they do require a mechanical shutter and the readout time overheads are often of the order 100% for one second cadence images, reducing much of the photoelectric efficiency gain. Our need for rapid observing cadence with minimal dead time drove us to use 35mm format interline CCDs that are commercially available in cameras from several vendors, because they can be read out while the next exposure is accumulating, eliminating readout overhead. Non-interline, front illuminated sensors were eliminated because the readout time overhead reduced the allowable exposure times, despite the availability of physically larger sensors.

Having settled on a family of detectors, we examined camera/telescope combinations to find the best etendue, collecting area (A) multiplied by the field of view (Omega), per dollar. The standout system in this analysis was a 14" Celestron Schmidt-Cassegrain optical tube with a HyperStar f/1.9 prime-focus corrector. Combined with an ON Semiconductor (formerly TrueSense (formerly Kodak)) KAF-16070 4864 x 3232 sensor with 7.4 micron pixels, this gives a 3° x 2° field of view with 2.23 arcsecond pixels, albeit with significant vignetting from the corrector in the corners of the field. These sensors are integrated into Finger Lakes Instruments Microline cameras, which were

chosen because they allowed a rapid dual amplifier read rate of 10MHz resulting in a 1Hz frame rate (principally limited by the USB2.0 bus) in a compact housing with integrated thermoelectric cooling. Because these cameras are operating at prime focus, the form factor is critical to preclude adding to the system obscuration, and the Microline camera adds only a small fraction compared to the corrector housing. The net result is an instrumental etendue of almost 0.5 m^2deg^2 for a 6 square degree FOV that can read out at 1 Hz with 11e- of read noise, essentially zero dead time between exposures, with parts available off-the-shelf for around $20,000.

We have deployed two of these systems in the Albuquerque metropolitan area, as shown in Figure 1. Siting telescopes this close to a major population center is not ideal and incurs a cost in detectivity, especially for the system within Albuquerque city limits, but it provides easily accessible systems for development and testing. The added noise from night sky is easily quantified and we can readily extrapolate the performance that would be expected from a dark sky site. Given the relatively small apertures involved and the rapid image cadence, a truly dark astronomical site (West Texas, Hawaii, Chile, etc.) is not crucial.

Each telescope and camera system is installed on a Paramount MX German Equatorial mount allowing precision pointing. These are attached to Parallax Instruments portable piers and installed in 7 foot diameter Astrohaven domes. The deployed systems in their domes are shown in Figures 2 and 3. Altogether - optical systems, mounts, domes and computers - the total cost per system is approximately $50,000, and the entire system can be deployed by a small team in about two hours, crate-to-sky.

Figure 1 – Google Earth views of the present deployment of JTMA's Proof-of-Concept LEO SSA Optical Systems. The systems are separated by 27 km enabling them to simultaneously observe the same volume of LEO and obtain range estimates based on parallax for objects detected with both systems.

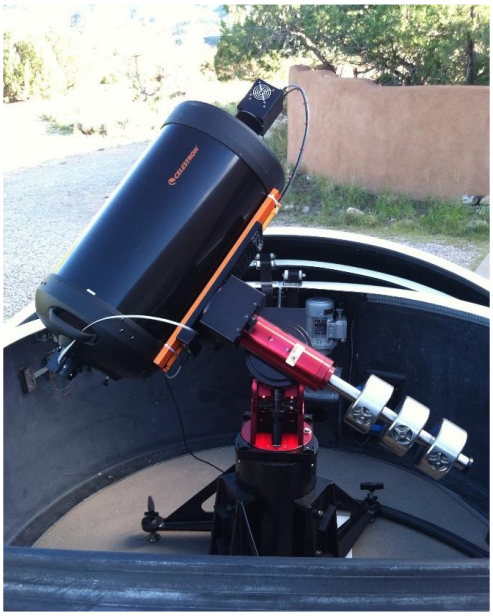

Figure 2 (left) and Figure 3 (right) – The northern JTMA Proof-of-Concept LEO SSA Optical Systems shown enclosed and opened to the sky awaiting twilight. The optical systems are 14" Celestron Schmidt-Cassegrain telescopes with Hyperstar prime focus wide field correctors installed. A FLI ML-16070 interline CCD provides a 3˚ x 2˚ field of view with 2.25" pixels and can be read out at 1 Hz with no deadtime between frames. The systems are enclosed in 7ft Astrohaven clamshell domes.

4. STREAK DETECTION – SOME SELECTED RESULTS

To enable rapid follow-up, the streak detection process needs to be fast - essentially real time (see Zimmer, Ackermann & McGraw 2013 [2] for more information on streak detection). Thus for our one frame per second acquisition cadence, the entire process must be similarly fast – a latency of a few seconds is acceptable but the throughput needs to be at the same rate as the data acquisition, one frame per second. We have parallelized our proprietary detection process for operation on Graphical Processing Units (GPU) and are working to move as much of the pre-processing pipeline as possible to the GPU as well. At present, the detection process takes two seconds per frame on a single NVidia GeForce 780 Ti (~$650 street price and falling), presently the most powerful single GPU available, while the pre-processing – background estimation, astrometry, star masking, etc. – takes about 3.5 seconds and is presently dominated by sequential CPU processing. Fortunately the price of GPUs keep falling and their speed keeps increasing which, combined with innate parallelism GPUs enable, means that fielding systems with 4 or more GPUs is affordable and easily implemented.

Each system produces 3600 images per hour, each of which is 16 megapixels, leading to a raw data rate of 115GB/hr. Each twilight observation period lasts roughly 2 hours, so the daily accumulation is 460GB per day in 14400 images when conditions are clear. Approximately one in 20 frames generates a detection above 6 σ, but this can vary between 100 – 600 detections per hour, with the latter corresponding to times when a HEO object crosses the FOV, which can be detected in hundreds of frames. The processing software is capable of making detections through thin clouds, but this impacts sensitivity both due to extinction of the signal light and also from elevated background noise.

The detection transform only determines the angle and intercept of the streak. Because we choose an exposure time to ensure that we capture streak endpoints for most trajectories through the field of view, we must extract the pixels corresponding to the most significant angle and intercept. Within that one dimensional set of values we determine the statistically most likely start and end of the streak.

We now present three sample object detections and show some of the analysis that is made possible by our telescopes and algorithms working together. ***Our systems make a few hundred detections per hour*** and we've picked a few that we have investigated further to demonstrate our system performance and features.

4.1 Detection of OV1-5

We start by describing detection of an "easy" object, OV1-5, one that is bright enough to be detected by just about any technique. Figure 4 shows a picture of one of the OV1 orbiters, which are about 1.5m long and 0.6m diameter cylinder. OV1-5 was launched in 1966 into a 1050km altitude orbit. Figure 5 shows the detection of OV1-5 with our northern system on June 25, 2014 at 03:35:43 UTC and Figure 6 shows the corresponding extracted along-track light curve.

Based on the photometry of stars in the FOV, the streak left by OV1-5 in one second measured 690,000 photo-electrons (430σ), so we estimate OV1-5 to have been 7.1 +/- 0.1 magnitude and was travelling at an apparent angular rate of ~1540″/s, which is consistent with its catalog altitude.

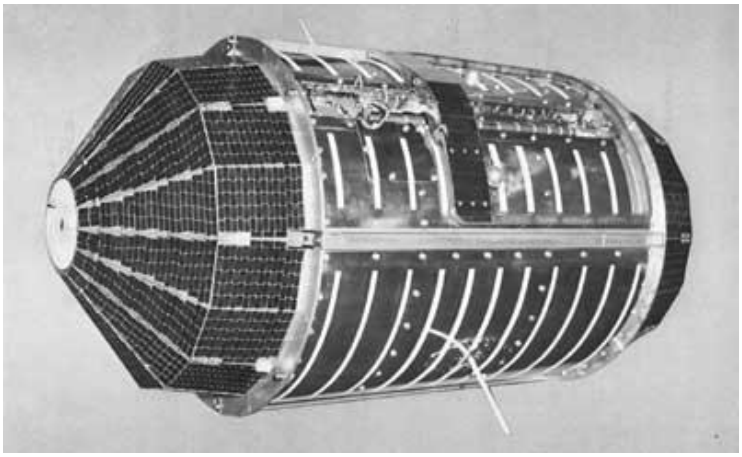

Figure 4 – Picture of an OV1 class object, estimated to be about 1.5m long.

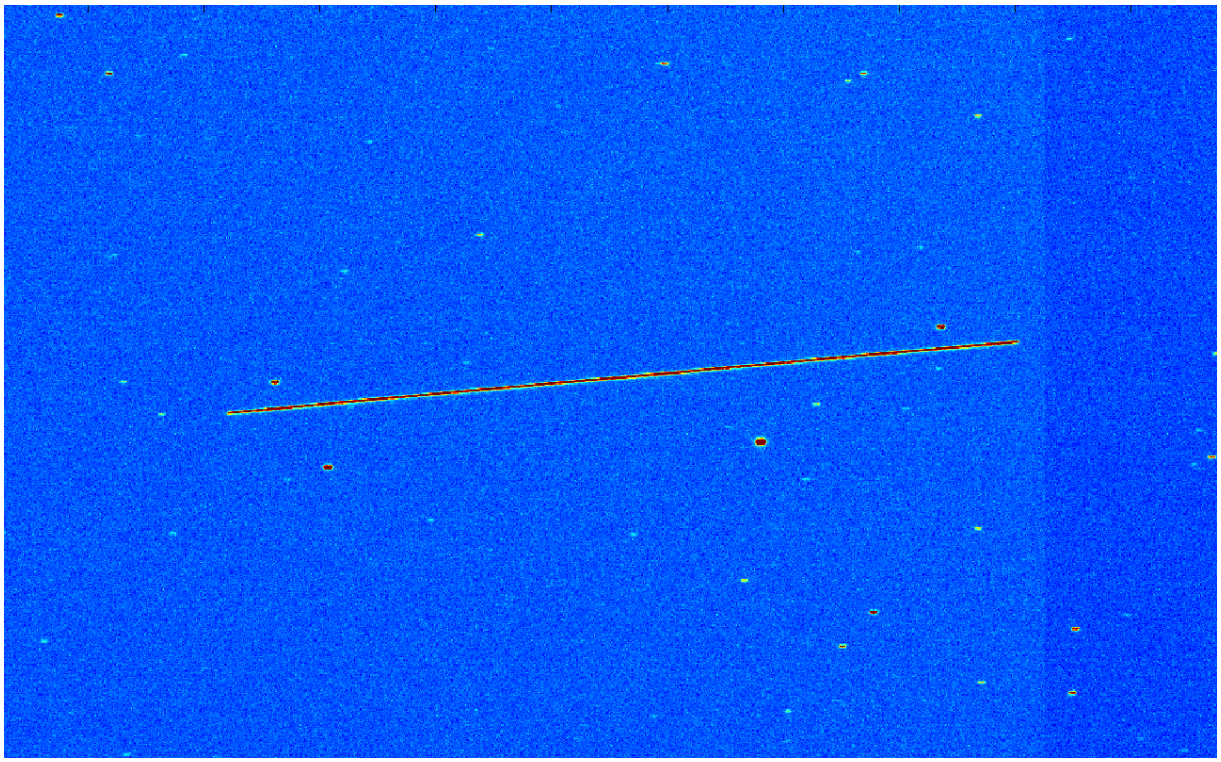

Figure 5 – This figure shows a 10' x 30' subsection of a raw one second exposure taken by the Placitas telescope capturing the streak from OV1-5. The boundary between the detector amplifiers is visible as a lower image gain on the right. Images are acquired with tracking motors off, so stars are streaked by one second of RA. The faintest stars visible here are between 15.5 and 16th magnitude.

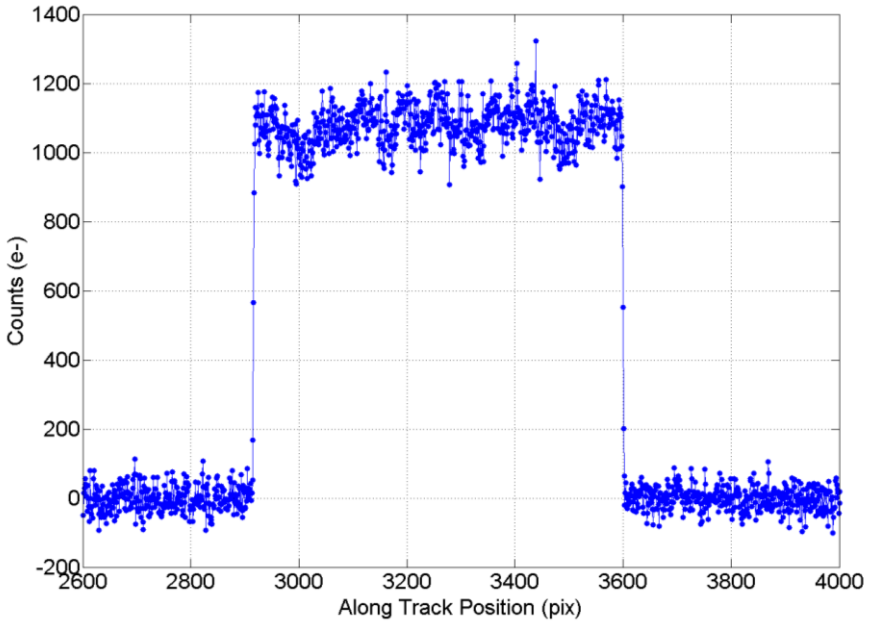

Figure 6 – This graph shows the along-track extracted profile for OV1-5.

We use the measured flux from nearby stars to estimate the magnitudes of our detected objects. Figure 7 shows the measured flux versus catalog magnitude for all the stars in the image from which the cutout in Figure 5 was extracted. There are typically a few thousand stars in the field, but can be as many as 20,000 near the galactic plane. The spread in flux vs. magnitude is a result of the strong vignetting of the Hyperstar corrector and the lack of any flat field correction, which is not performed because the primary goal of this work is detection, not accurate photometry. On average though, a 12th magnitude object deposits ~8500 e-/s and we use this as a rough guide for estimating object magnitudes. For more precise values, we evaluate stars near the object streak.

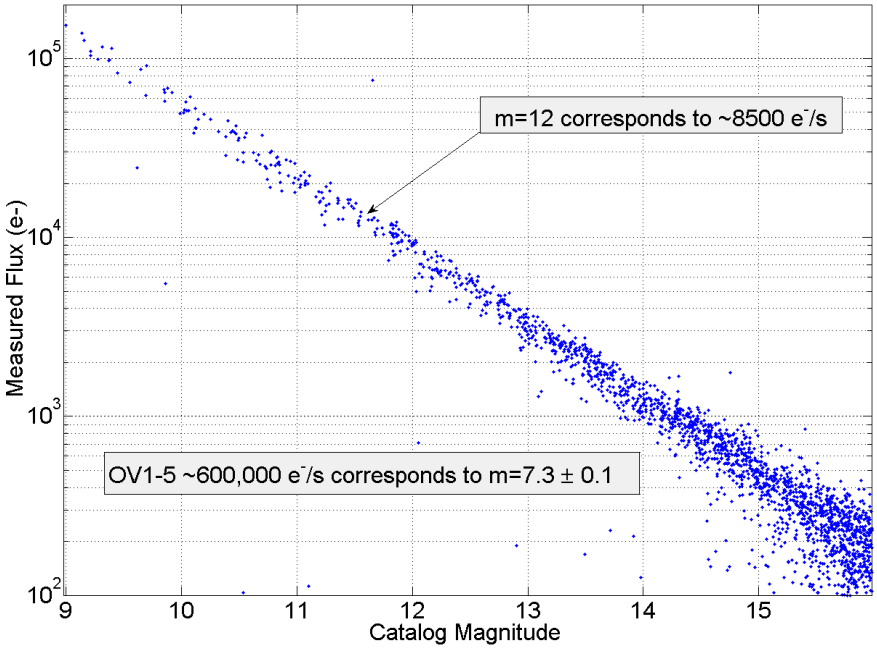

Figure 7 – Quick-look photometry of field stars is plotted versus catalog magnitude in the entire image for the cutout shown in Figure 5. From plots such as these, we estimate that a 12th magnitude object deposits 8500 e-/s on average, though this depends strongly on where the object is in the field due to strong vignetting of the Hyperstar corrector.

4.2 Detection of ~20cm Unknown Object at ~600km altitude

OV1-5 is very bright, so it is no surprise that it is easily detected with high signal to noise. More interesting are the many objects we can detect that are close to our detection threshold. One such example is shown in Figures 8 and 9. This object has no counterpart in the publically available Space Track catalog. For this object, we measured 12,500 photoelectrons along a path 1220 pixels long – about 10 per pixel where the noise per pixel (sky and read noise) is 15 electrons – see Figure 10. This corresponds to an apparent angular rate of 2720 arcseconds per second, which corresponds to a circular orbit altitude of approximately 600km. The apparent magnitude of this object is 11.6 +/- 0.2 and which at this range, corresponds to an 18-20cm diameter diffuse sphere with albedo of 0.12.

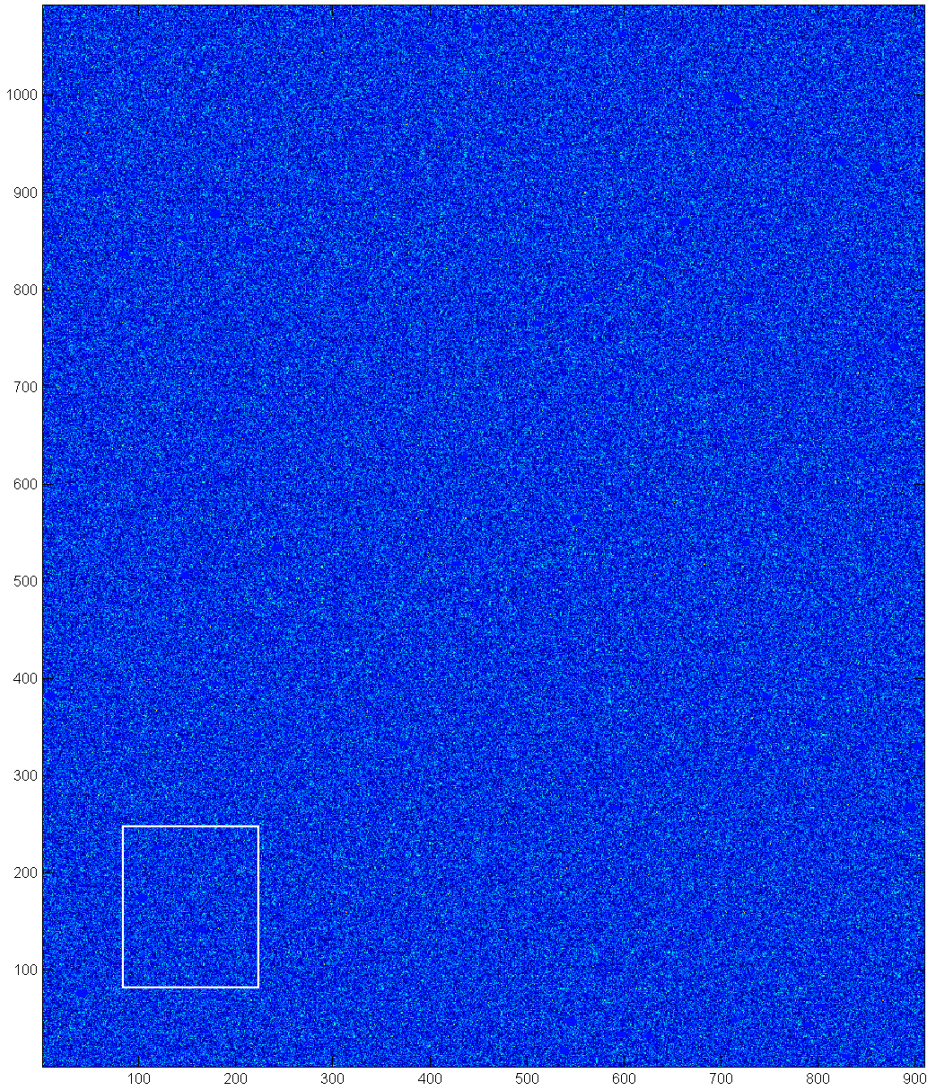

Figure 8 – 40' x 30' Image subsection showing the detection of an unknown faint object estimated to be roughly 20cm in size and in a 600km altitude orbit, assuming a diffuse sphere with 0.12 albedo and a circular orbit. The visible points along the streak are 0.7 σ above the background. The white square shows the region that is zoomed in for Figure 9. The color scale in both figures is shaded to show dark blue as -2σ and red as +5σ of the background noise distribution.

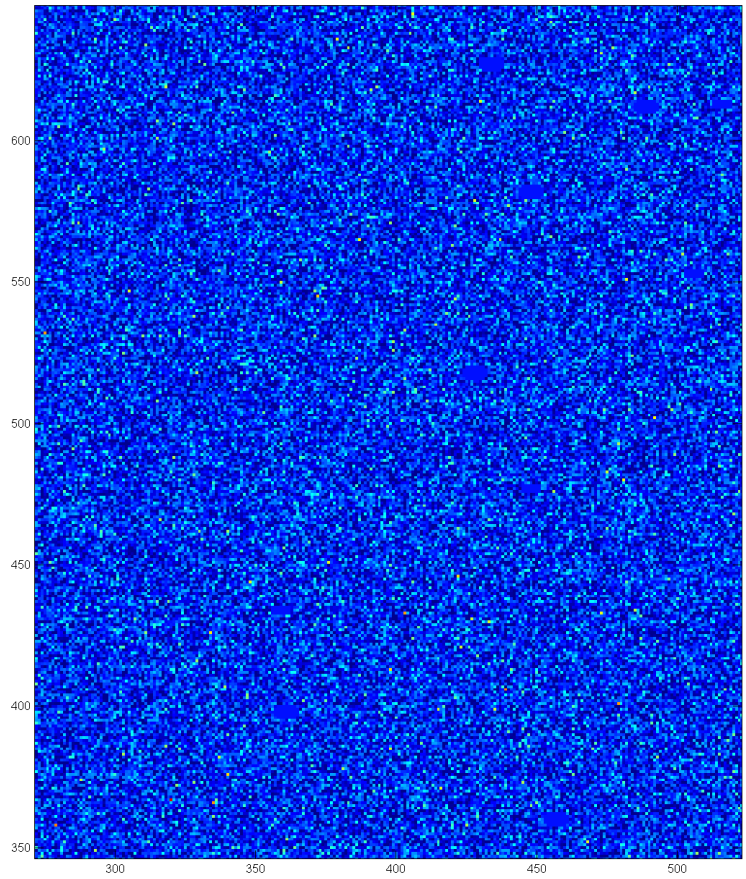

Figure 9 – Zoomed in region of Figure 8.

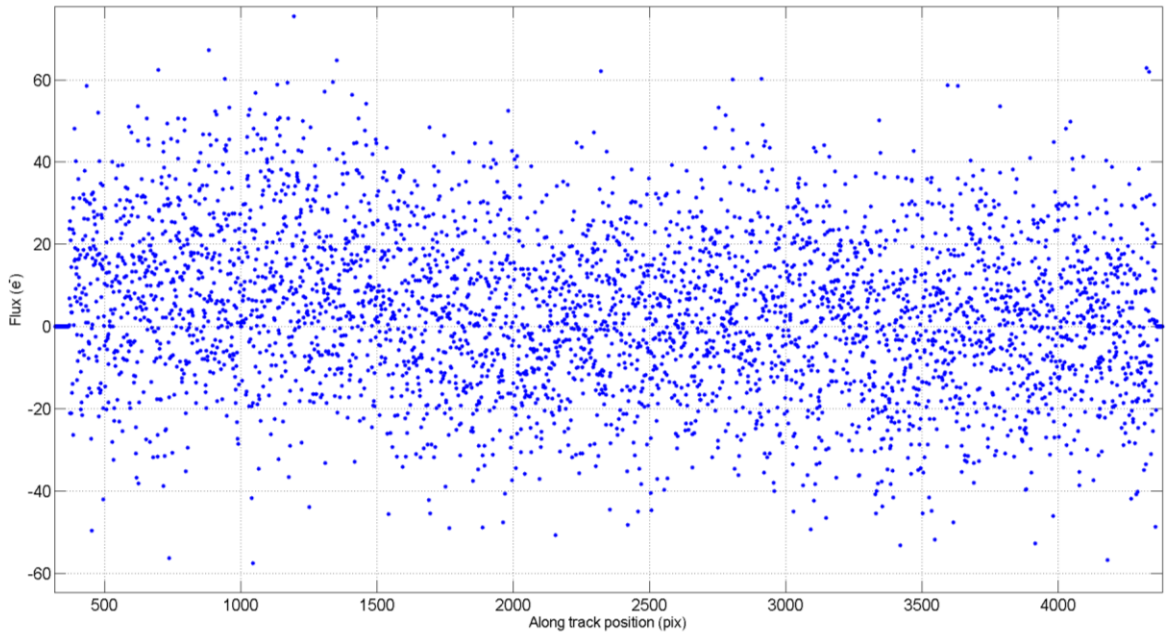

Figure 10 – Our detection system automatically generated this along-track intensity profile of the object in Figures 8 & 9. Summed along the path, the object is detected at 8.6 σ. Optimum significance is found between pixel location 600 and 1800, where the object is 14.9 σ above the background.

This object was detected by our automated processing system as 8.6 σ above the system noise, which implies the limiting magnitude in this case was approximately 12, or a ~15cm object. Once the object is found, we can extract it for optimal signal-to-noise, which in this case is 14.9 σ, which means the optimal limiting magnitude is 12.6, corresponding to a roughly 11cm object at 600km.

4.3 Detection of an Unknown object at 4500 km

Our last sample detection exhibits some interesting features. Figure 11 shows cutouts of the 15 frames in which the object was detected and Figure 12 shows extracted along-track intensity profiles. Unlike the previous two examples, this object is moving much more slowly, about 460”/s. We can use the technique detailed by Michael Earl (2006 [3]) for estimating circular orbit parameters from zenith pointing observations. These observations corresponding to a circular orbit at 4435km with an inclination of 105 degrees.

We were able to further refine this using STK [4] to roughly match the observations. This allowed us to refine the inclination to 105 ± 0.1 degrees. This combination of altitude and inclination is an interesting combination and because there is no plausible match in the publically available Space-Track [5] catalog.

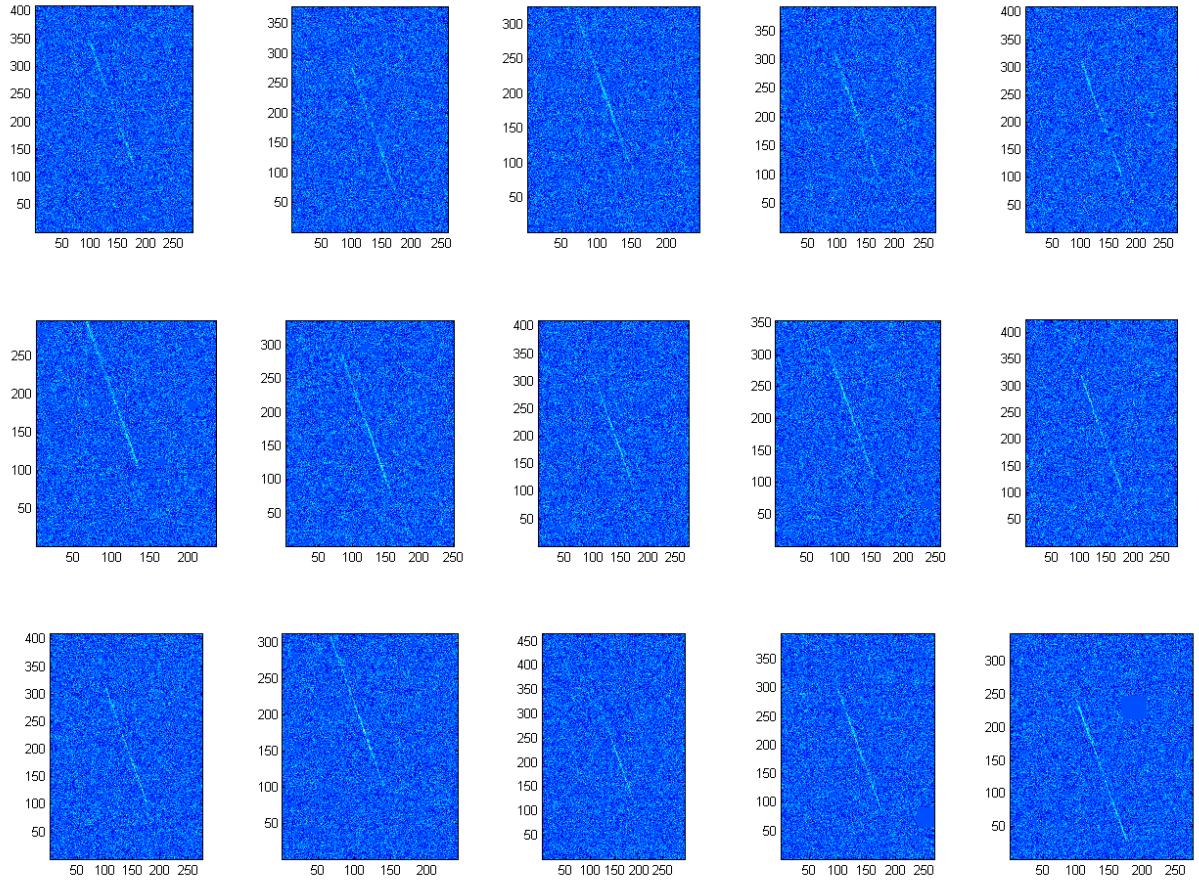

Figure 11– 15 x 10 arcminute cutouts of the 15 consecutive detections, with time progressing in one second increments left-to-right then top-to-bottom, of an unknown object with estimated altitude of 4500km as it crossed the field of view of our system. It is apparent even from these cutout images that the object is changing brightness, sometimes within a one second exposure.

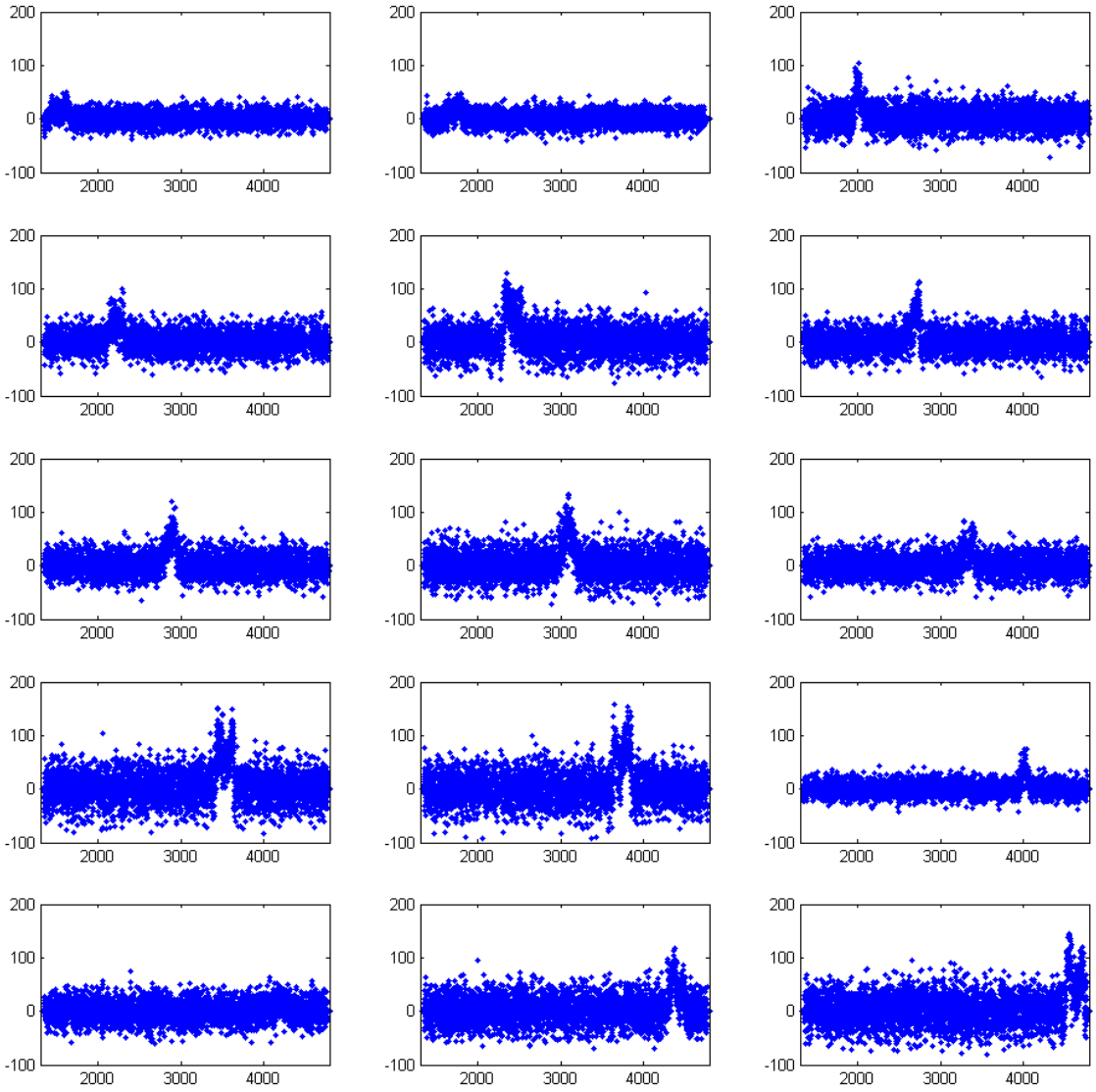

Figure 12 – Extracted along-track intensity profiles corresponding to the detections shown in Figure 11. The varying levels of background noise are due to the streak being extracted across more significant pixels in the cross track direction – when it is faint, as in the first two frames, it is only significant in a one pixel wide path. As it brightens, it covers a wider path, and while the noise is increased, the detection significance is still higher, but leads to a small aperture correction between brighter and fainter detections.

This object is also interesting because its intensity is modulating rapidly, which is apparent in both Figures 11 and 12, both between adjacent and even within exposures. Figure 13 plots the magnitude estimate for each frame. While some of the variation can be explained by instrumental effects, the object is clearly changing apparent brightness by more than a magnitude on one second and faster timescales. When it is bright, it is equivalent to a 1.4m diameter diffuse reflector with albedo of 0.12. When it is faint, the effective diameter drops to 0.6m.

We are hoping to detect this object again. We have a larger time window for this altitude range because terminator conditions last much longer than for lower LEO orbits, thus we'll target some longer observation windows when this object might again be visible.

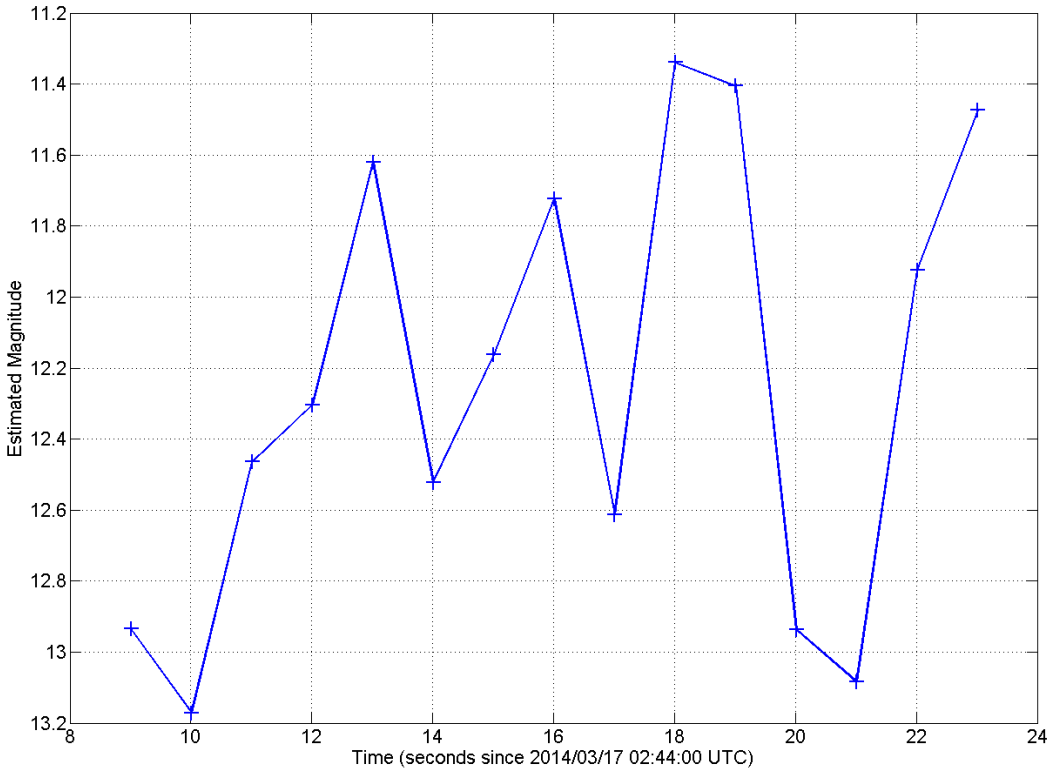

Figure 13 – Estimated object magnitude for each of the 15 exposures captured while it crossed the FOV. The large jump between exposures 11 and 12 constitutes a change of almost a factor of 4 in brightness in one second.

5. PARALLAX RANGE TO LEO OBJECTS

We've chosen to deploy the two systems at sites separated by roughly 27km enabling overlapping fields of view in the LEO volume above and between them. Using optical parallax to measure range to satellites has been discussed previously (Earl 2005 [6], McGraw et al. 2008 [7]). Our most frequent alignment and the one used for the results presented here is with the two telescopes pointed toward each other in azimuth and tilted from the zenith by about 0.8 degrees. In this configuration, the converging FOVs start to coincide at 500km, achieve maximum overlap around 1000km and diverge again completely at 2000km, a configuration chosen to cover objects in the populations at 800km and also those at 1400km.

The 27km baseline produces an apparent parallax with respect to background stars of approximately $\tan^{-1}(27/D)$, where D is the distance in km from the midpoint between the two systems to the object being observed. When D is 1000km, the parallax angle is roughly 1.5 degrees. In detail, the trigonometry is more complex, but the principle is the same. Each system measures an apparent right ascension (RA) and declination (Dec) to the object as a function of time. Those two lines of sight to the object converge at the location the object was at that time. Because of measurement errors, the lines of sight never truly cross, but their point of closest approach is calculable with simple geometry [8]. The observations at the two sites are synchronized in time so that end point times can be used as a common reference.

Figure 14 shows a schematic of the observation geometry along with sample streaks from OV1-5, the same object discussed in Section 4.1. We are using this object as our example because it is bright, thus having a high signal-to-noise along the streak, its orbit altitude is in the middle of our overlap volume and has moderate inclination, crossing our fields of view nearly east to west, perpendicular to the baseline separating our two telescope systems.

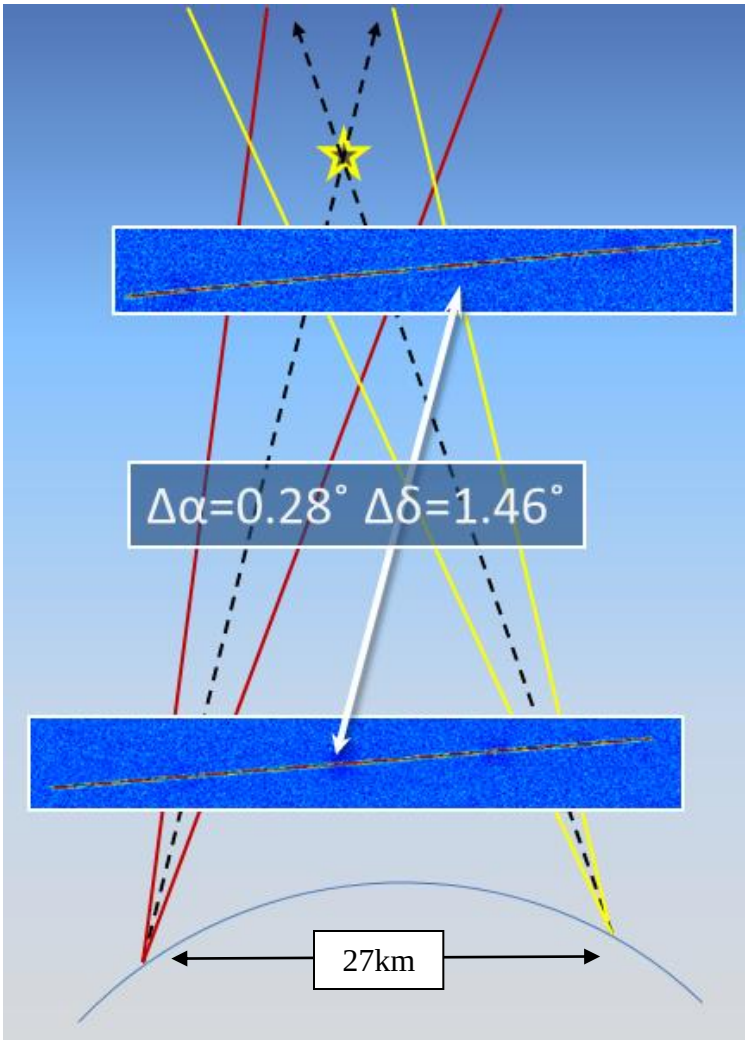

Figure 14 – Schematic drawing of the parallax geometry with estimated parallax angles in RA and Dec.

Because of this geometry, we are able to measure positions in the cross-track direction very well, but less so in the along-track direction. Moreover, the long lever arm of the parallax measurement means that small angle measurement errors are amplified in the range direction. For example, in the cross-track direction, a change of one pixel is simply the angle subtended by the pixel time the distance to the object, which is roughly 12m for a 1000km object with our configuration. In range, one pixel error leads to a range estimate error of the order 500m.

This configuration is shown in Figures 15 and 16 where our parallax measured position of OV1-5 is compared to the SGP4 propagated (using STK) Space-Track TLE from the observation epoch. The error ellipses show measurement uncertainty from each telescope having a roughly ½ pixel (1.1 arcsecond) measurement uncertainty in each. Figure 15 shows the positions in a 3D plot of Earth Centered Inertial coordinates (in km) as viewed from above the line of sight to OV1-5 from the telescope sites. Figure 16 shows the same information but along the line of sight. The range estimates are consistent with the TLE estimate while the cross-track direction shows a systematic offset of about 100m. Because that offset is due to a declination difference, we believe it to be real and significant and within the range expected of TLE/SGP4 predictions.

Our astrometric fit residuals are on the order of 0.1 pixel (0.25-0.3 arcseconds), dominated by the distortion of the Hyperstar corrector and seeing, thus our position measurements should be significantly better than this. We are actively studying this. At the sub-pixel level, many more effects need to be considered including timing offsets and jitter, position measurement along the streaks and relativistic effects. We believe parallax measurement such as these should produce position measurements to better that 100m in range and a few meters cross-track.

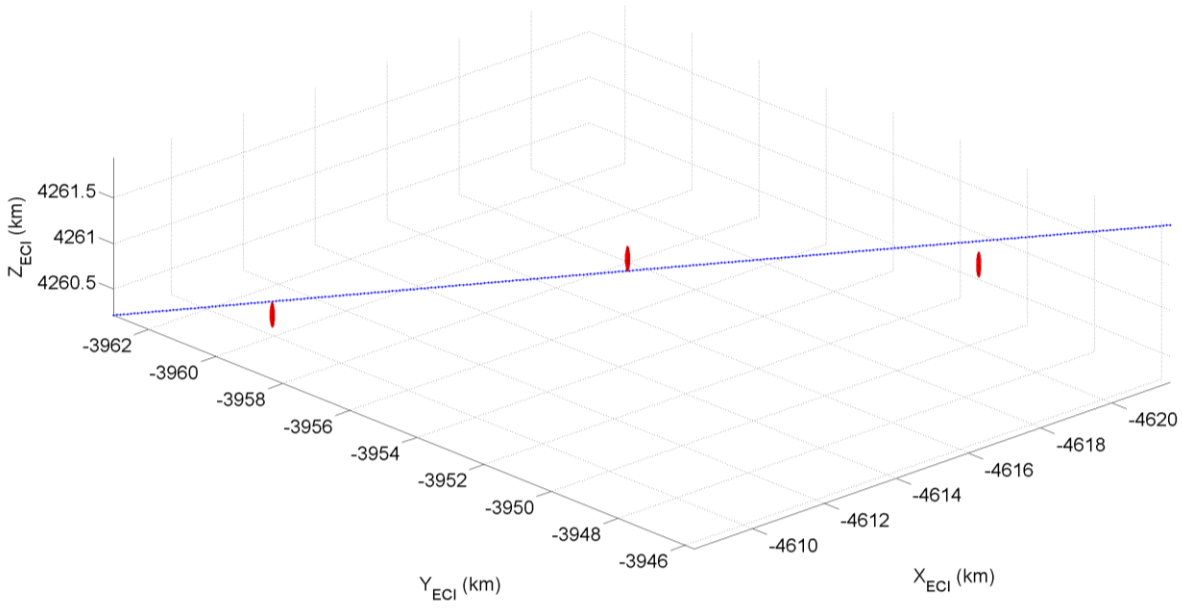

Figure 15 – Parallax measured positions in time for the three streak endpoint pairs of OV1-5 are shown as red ellipsoids with the ellipse dimensions indicating estimated measurement errors. In this figure, the view is from above and perpendicular to the line of sight from the telescope systems to OV1-5 to show range errors of approximately +/- 250m.

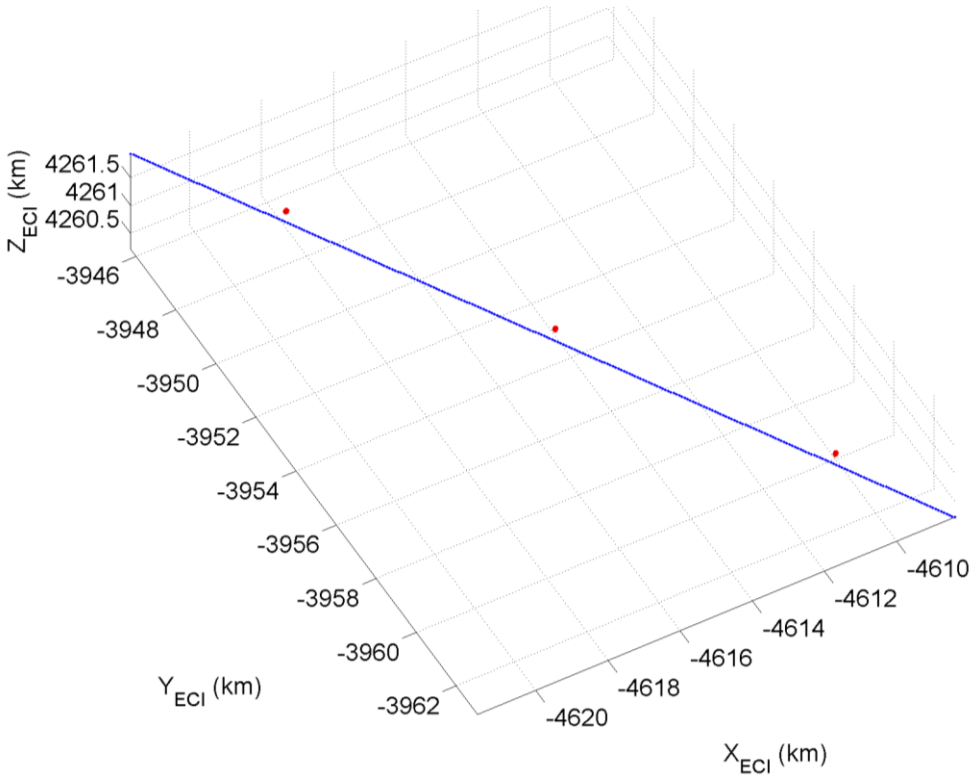

Figure 16 – Same data are plotted as in Figure 15, but from the view along the line of site from OV1-5 back to the telescope systems. The smaller cross-track uncertainties are shown and the systematic offset of ~100m is thought to be real and significant.

6. POTENTIAL OF SMALL TELESCOPES FOR OPTICAL SSA OF LEO

We've built two small wide-field optical systems now deployed in the Albuquerque, NM area to demonstrate the immense potential of small telescopes for LEO SSA. These systems couple high cadence, zero dead time imagery with advanced GPU-based streak detection algorithms to find and measure LEO objects, both known and heretofore unknown. We have demonstrated detection, photometry, and astrometry all produced in near real time, as well as parallax range estimates for an object measured simultaneously by both systems. These sample detections are but a few of the hundreds we obtain per operational night and continue to examine and test.

In addition to the work shown here, we have also developed an advanced detection algorithm that is more effective at finding short streaks, such as those from higher altitude objects (MEO, GEO, HEO, GTO, etc.). This techniques approaches the optimal extraction limit at an increased, but still practical, cost of computational power. Our performance models (see [2]), which have been largely verified by the measurements we are presently making, indicate that by applying these techniques to appropriately acquired data from large aperture, wide-field telescopes (e.g. Pan-STARRS, SST) could push the limiting magnitude, and therefore size limits, for streak detection down below 5cm objects at 1000km, possibly as low as 2cm for SST – possibly 18th magnitude!

Large wide-field telescopes are not likely to be deployed in large numbers for SSA in the near future, but small telescopes could be. Figure 16 shows a notional optical fence made up of 100 small telescopes with 5 x 2.5 degree FOVs aligned in fan beams from 8 well-chosen sites in along desert southwest. We think that this is a practical and affordable solution to LEO SSA and the work presented here shows that the basic principles are correct and effective.

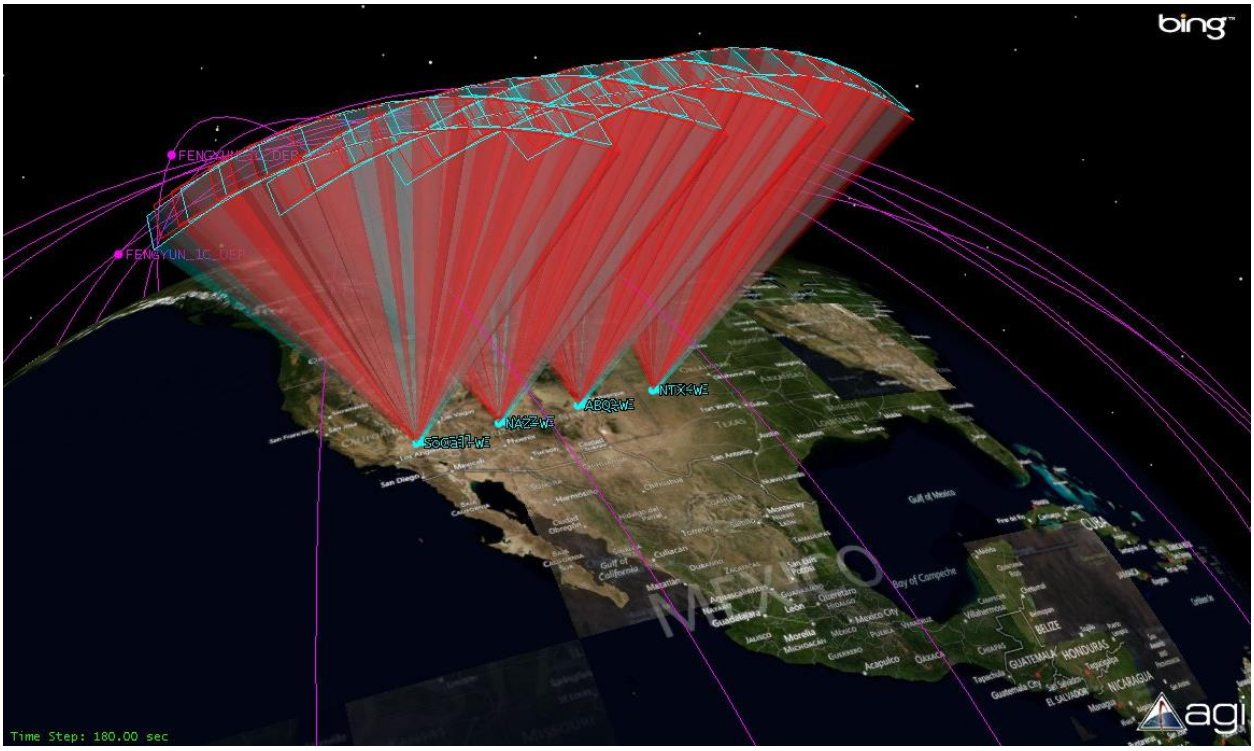

Figure 16 – Notional optical fence showing 100 telescopes covering a similar volume as the old space fence. The sites and telescope configurations are chosen to enable parallax range measurements of moderate to high inclination LEO objects that pass over the US, with complete coverage down to 450km altitude and of eight congressional districts in four states. A system such as this is capable of providing effective and affordable SSA of a significant and important fraction of the LEO volume.

7. ACKNOWLEDGEMENTS

This work has been supported in part by the Air Force SBIR program under contract number FA9451-13-C-0092.

8. REFERENCES

[1] Ackermann, Mark R., McGraw, John T., Martin, Jeffrey B., Zimmer, Peter C. 2003, "Blind Search for Micro Satellites in LEO: Optical Signatures and Search Strategies*", Proceedings of the 2003 AMOS Technical Conference*, also published as Report No.: SAND2003-3225C, Sandia National Laboratories, Albuquerque, NM (USA), September 2003.

[2] Zimmer, Peter C., Ackermann, Mark R., McGraw, John T. "GPU Accelerated Faint Streak Detection for Uncued Surveillance of LEO*", Proceedings of the 2013 AMOS Technical Conference*, 2013.

[3] Michael A. Earl, "Determining the Orbital Height of a Low-Earth-Orbiting Artificial Satellite Observed near the Local Zenith," *Journal of the Royal Astronomical Society of Canada* 100, 199 (2006).

[4] Satellite Tool Kit by Analytical Graphics Inc. (www.agi.com)

[5] www.space-track.org

[6] M. A. Earl, "Determining the Range of an Artificial Satellite Using its Observed Trigonometric Parallax," *Journal of the Royal Astronomical Society of Canada* 99, 50 (2005).

[7] J. McGraw, M. Ackermann, P. Zimmer, S. Taylor, J. Pier, and B. Smith, "Angles and Range: Initial Orbital Determination with the Air Force Space Surveillance Telescope (AFSST)," presented at Advanced Maui Optical and Space Surveillance Technologies Conference, 2008, 48.

[8] James Foley, Andries van Dam, Steven Feiner & John Hughes, "Clipping Lines" in *Computer Graphics (3rd Edition)* 2013.